

Robust integral formulations for electromagnetic scattering from three-dimensional cavities

Jun Lai,^{*} Leslie Greengard,[†] and Michael O’Neil[‡]

January 20, 2022

Abstract

Scattering from large, open cavity structures is of importance in a variety of electromagnetic applications. In this paper, we propose a new well conditioned integral equation for scattering from general open cavities embedded in an infinite, perfectly conducting half-space. The integral representation permits the stable evaluation of both the electric and magnetic field, even in the low-frequency regime, using the continuity equation in a post-processing step. We establish existence and uniqueness results, and demonstrate the performance of the scheme in the cavity-of-revolution case. High-order accuracy is obtained using a Nyström discretization with generalized Gaussian quadratures.

1 Introduction

The computation of electromagnetic wave propagation in the presence of large, open cavities is an important modeling task. It is critical, for example, in understanding the effect of exhaust nozzles and engine inlets on aircraft, as well as surface deformations in automobiles and other land-based vehicles [4, 8, 29, 31, 33]. The presence of such structures plays a dominant role in both the near field, where electromagnetic interference is of concern, and in the far field, where the radar cross-section can be used for identification and classification (including stealth-related calculations). Fast and accurate solvers to simulate such scattering phenomena are essential for both design optimization and verification.

A variety of numerical methods have been proposed to solve such scattering problems. Largely speaking, they fall into two categories. The first is direct numerical simulation using finite difference [8], finite element [33], mode-matching [5] and boundary integral methods [8, 38]. The second is asymptotic methods, including Gaussian beam approximations [13] and physical optics-based schemes [32]. The latter methods tend to work well at very high frequencies in the absence of multiple near-field scattering events, and are generally not well suited for high-precision calculations in geometrically complex environments. Solving the governing Maxwell equations using finite difference and finite element methods, on the other hand, requires the discretization of an unbounded domain. In practice, these methods must either employ approximate outgoing

^{*}Courant Institute, New York University, New York, NY. Email: lai@cims.nyu.edu

[†]Courant Institute, New York University, and Simons Center for Data Analysis, Simons Foundation, New York, NY. Email: greengard@cims.nyu.edu

[‡]Courant Institute and Tandon School of Engineering, New York University, New York, NY. Email: oneil@cims.nyu.edu

boundary conditions to mimic the radiation condition at infinity, or be coupled with a boundary integral representation beyond some distance so that the radiation condition is satisfied exactly. In the present work, we will focus on boundary integral equation methods since they are free from grid-based numerical dispersion, can achieve high-order accuracy in complex geometry, and require degrees of freedom only on the boundary of the scatterer itself, greatly reducing the number of unknowns. The Green’s function used to represent the solution satisfies the outgoing (radiation) condition exactly. Existing integral representations for cavity problems, however, generally yield integral equations of the first-kind [1]. First-kind equations can lead to ill-conditioned discrete linear systems, especially if substantial mesh refinement is required. Refined meshes may be needed, for example, to resolve geometric singularities. Furthermore, several existing formulations also suffer from *spurious resonances*, including those of mixed first-/second-kind systems [38]. Finally, because of the nature of the dyadic Green’s function for the electric field, standard methods based on discretizing the physical electric current also suffer from low-frequency breakdown [16, 40]. This behavior is discussed in more detail below.

In this paper, we propose a new representation of the scattered field that leads to a well-posed (resonance-free) integral equation which is immune from low-frequency breakdown. This allows for a stable numerical discretization along arbitrarily adaptive meshes. In our numerical examples, using the the fact that the scatterer (i.e. the cavity) is axisymmetric permits us to use separation of variables in cylindrical coordinates, applying the Fourier transform in the angular (azimuthal) variable. This procedure leads to a sequence of uncoupled two-dimensional boundary integral equations on the generating curve that defines the cross-section of the boundary of the scatterer (see Fig. 3). There are various numerical technicalities associated with implementing body-of-revolution integral equation solvers, and we do not seek to review the substantial literature here. We instead refer the reader to [23, 24, 28, 34, 39] and the references therein. A concise overview of the discretization and resulting solver is given in Section 5. Similar high-order techniques have been applied to solve the Helmholtz equation on surfaces of revolution [23, 24, 34, 39] and the full Maxwell equations (for closed-cavity resonance problems) in [25].

Due to the applicability of cavity scattering in physics and engineering, there has been much work dedicated to both the mathematical and numerical aspects of the problem. The well-posedness of the (forward) scattering problem is discussed in [1, 2] in the case of the two-dimensional problem, and in [3] for the three-dimensional case. The paper [9] provides the explicit dependence of the scattered field on the wavenumber in the high-frequency context. In [4, 30], the authors studied uniqueness and stability issues for the inverse problem, where one seeks to recover the shape of an unknown cavity using near-field data. The corresponding optimal design problem, i.e. to find a cavity shape that minimizes the radar cross section, under certain constraints, is discussed in [6, 7] in the two-dimensional setting.

An outline of the paper follows: Section 2 provides a detailed introduction to the problem of scattering from an open cavity and proposes an integral representation that leads to a well conditioned integral formulation. In Section 3, we prove that this integral equation has a unique solution for a given incident field. In Section 4, we show how to avoid low-frequency breakdown merely by the use of various vector identities and physical considerations. In Section 5, we briefly discuss the

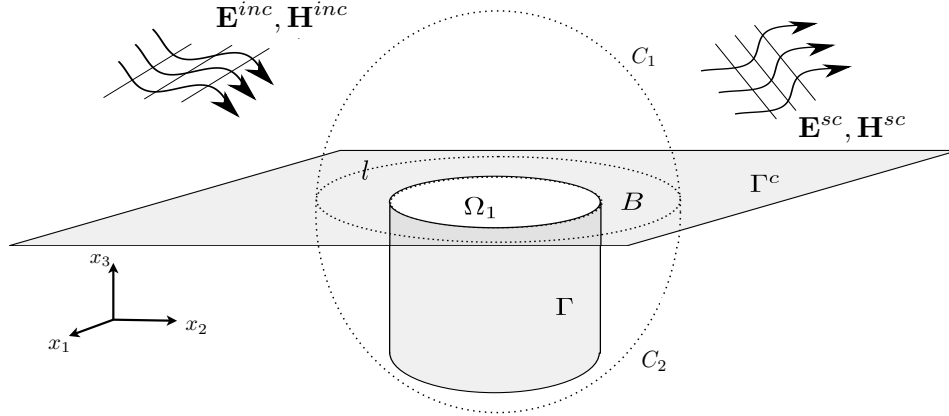


Figure 1: A cavity Ω_1 in a perfectly conducting half-space $x_3 \geq 0$, with boundary Γ . The surfaces C_1 and C_2 define the two halves of a sphere C which is sufficiently large to contain the cavity and a finite buffer region, denoted by B , in the x_1x_2 -plane beyond the edge of the cavity. The curve ℓ denotes the outer edge of the buffer region B . The unbounded half-space boundary outside of C is denoted by Γ^c .

separation of variables solver for axisymmetric cavities, and then illustrate its accuracy and stability in Section 6. Section 7 contains a brief discussion of open problems and some concluding remarks.

2 Mathematical formulation of the scattering problem

Suppose now that a perfectly conducting cavity Ω_1 extends into the lower half-space $x_3 < 0$, as depicted in Figure 1. See the caption of Figure 1 for a description of the geometrical setup. The region in the lower half-space with boundary $\Gamma \cup B \cup \Gamma^c$ is assumed to be perfectly conducting. Given a time harmonic incident field $(\tilde{\mathbf{E}}^{inc}, \tilde{\mathbf{H}}^{inc})$ with an implicit time dependence of $e^{-i\omega t}$, we seek to find the scattered field $(\tilde{\mathbf{E}}^{sc}, \tilde{\mathbf{H}}^{sc})$ so that the total field

$$\tilde{\mathbf{E}} = \tilde{\mathbf{E}}^{inc} + \tilde{\mathbf{E}}^{sc}, \quad \tilde{\mathbf{H}} = \tilde{\mathbf{H}}^{inc} + \tilde{\mathbf{H}}^{sc}$$

satisfies the the Maxwell equations

$$\begin{aligned} \nabla \times \tilde{\mathbf{E}} - i\omega\mu \tilde{\mathbf{H}} &= 0, \\ \nabla \times \tilde{\mathbf{H}} + i\omega\varepsilon \tilde{\mathbf{E}} &= 0 \end{aligned}$$

for $\mathbf{x} \in \mathbb{R}^{3+} \cup \Omega_1$. The material parameters are given by ε , the electric permittivity, and μ , the magnetic permeability. Assuming ε and μ are constant, it is convenient to denote suitably normalized fields by $\mathbf{E} = \sqrt{\varepsilon}\tilde{\mathbf{E}}, \mathbf{H} = \sqrt{\mu}\tilde{\mathbf{H}}$, etc., leading to a simpler form of Maxwell's equations

$$\begin{aligned} \nabla \times \mathbf{E} - ik \mathbf{H} &= 0, \\ \nabla \times \mathbf{H} + ik \mathbf{E} &= 0, \end{aligned} \tag{2.1}$$

where $k = \omega\sqrt{\mu\varepsilon}$ is known as the wavenumber. We assume that $\Re(k) > 0$ and $\Im(k) \geq 0$. For perfect conductors, it is well-known [37] that the tangential electric field must satisfy the boundary

conditions

$$\mathbf{n} \times \mathbf{E} = \mathbf{0} \quad \text{on } \Gamma^c \cup \Gamma, \quad (2.2)$$

where \mathbf{n} is the interior normal direction along $\Gamma^c \cup \Gamma$. The scattered field must also satisfy the Silver-Müller radiation condition:

$$\lim_{|\mathbf{x}| \rightarrow \infty} \frac{1}{|\mathbf{x}|} \left(\mathbf{H}^{\text{sc}} \times \frac{\mathbf{x}}{|\mathbf{x}|} - \mathbf{E}^{\text{sc}} \right) = 0. \quad (2.3)$$

Remark 1. In the following derivations and computations, we assume that the incident field $(\mathbf{E}^{\text{inc}}, \mathbf{H}^{\text{inc}})$ is defined so that it satisfies not only Maxwell's equations, but also the tangential boundary condition $\mathbf{n} \times \mathbf{E}^{\text{inc}} = \mathbf{0}$ on the entire half-space $x_3 = 0$. This is easy to accomplish by reflection and discussed in more detail in Section 6.

Before discussing the solution of the cavity problem itself, we introduce some necessary notation. Given a tangential vector field \mathbf{j} along some surface Γ , the *vector potential* is defined by the single-layer potential

$$\mathcal{S}_\Gamma \mathbf{j}(\mathbf{x}) = \int_\Gamma G(\mathbf{x}, \mathbf{y}) \mathbf{j}(\mathbf{y}) dA_y, \quad (2.4)$$

where $G(\mathbf{x}, \mathbf{y})$ is the Green's function for the three-dimensional Helmholtz equation

$$G(\mathbf{x}, \mathbf{y}) = \frac{e^{ik|\mathbf{x}-\mathbf{y}|}}{4\pi|\mathbf{x}-\mathbf{y}|}. \quad (2.5)$$

It is well known [37] that in the case where $\mathbf{j} = \mathbf{J}$, a physical electric current, then the corresponding electric and magnetic fields generated by \mathbf{J} are given by

$$\begin{aligned} \mathbf{E} &= -\frac{1}{ik} \nabla \times \nabla \times \mathcal{S}_\Gamma \mathbf{J}, \\ \mathbf{H} &= \nabla \times \mathcal{S}_\Gamma \mathbf{J}. \end{aligned} \quad (2.6)$$

Likewise, if $\mathbf{j} = \mathbf{M}$, a surface *magnetic current*, then the electric and magnetic fields induced by \mathbf{M} are given by the *vector anti-potentials*

$$\begin{aligned} \mathbf{E}^a &= \nabla \times \mathcal{S}_\Gamma \mathbf{M}, \\ \mathbf{H}^a &= \frac{1}{ik} \nabla \times \nabla \times \mathcal{S}_\Gamma \mathbf{M}. \end{aligned} \quad (2.7)$$

Due to the linearity of Maxwell's equations, any linear combination of electric current-like variable \mathbf{j} and magnetic current-like variable \mathbf{m} will generate a Maxwellian field

$$\begin{aligned} \mathbf{E}(\mathbf{j}, \mathbf{m}) &= \alpha \mathbf{E}(\mathbf{j}) + \beta \mathbf{E}^a(\mathbf{m}), \\ \mathbf{H}(\mathbf{j}, \mathbf{m}) &= \alpha \mathbf{H}(\mathbf{j}) + \beta \mathbf{H}^a(\mathbf{m}). \end{aligned} \quad (2.8)$$

Only when $\beta = 0$ does \mathbf{j} correspond directly to the *physical* electric current. In order to develop a well-conditioned integral equation for the cavity problem, we will make use of both potentials and anti-potentials in the representation. Boundary conditions will then determine the values of \mathbf{j} and \mathbf{m} . Such an approach is sometimes called the *indirect-method* since the unknowns are not the fields themselves.

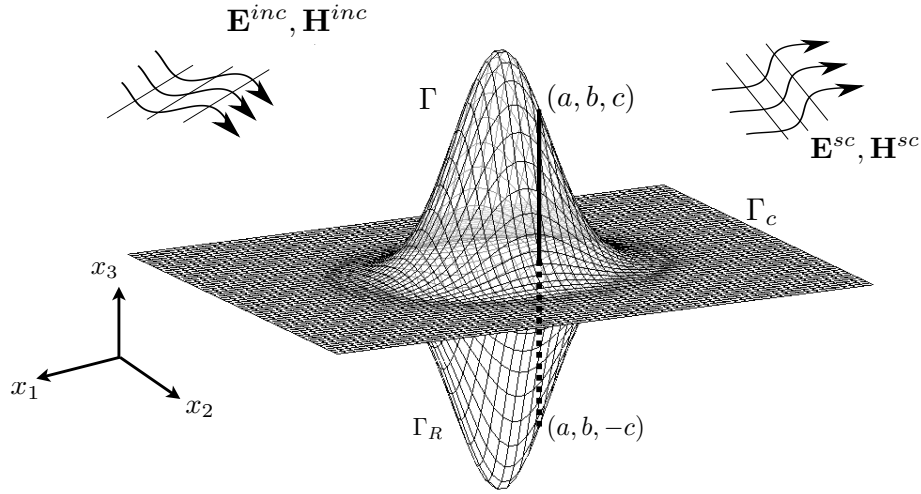


Figure 2: A bump Γ on a perfectly conducting half-space $x_3 \geq 0$. Γ_R denotes the reflection of the bump across the x_1x_2 -plane. The unbounded half-space boundary beyond Γ is denoted by Γ_c .

2.1 A simpler problem: The bump

It is first worth considering the simpler problem where the defect in the half-space boundary is a compactly-supported *bump* instead of a cavity (Fig. 2). This problem can be solved using standard integral equations and the method of images. We need only satisfy boundary condition (2.2), which we write in the form:

$$\mathbf{n} \times \mathbf{E}^{\text{sc}} = -\mathbf{n} \times \mathbf{E}^{\text{inc}}. \quad (2.9)$$

Since, by assumption, $\mathbf{n} \times \mathbf{E}^{\text{inc}} = \mathbf{0}$ away from the bump, we need only satisfy condition (2.9) on the bump itself as long as we can construct a representation for \mathbf{E}^{sc} that satisfies $\mathbf{n} \times \mathbf{E}^{\text{sc}} = \mathbf{0}$ away from the bump. To this end, we can define

$$\mathbf{E}^{\text{sc}} = \nabla \times \mathcal{S}_\Gamma \mathbf{M} + \nabla \times \mathcal{S}_{\Gamma_R} \mathbf{M}_R \quad (2.10)$$

and

$$\mathbf{H}^{\text{sc}} = \frac{1}{ik} \nabla \times \nabla \times \mathcal{S}_\Gamma \mathbf{M} + \frac{1}{ik} \nabla \times \nabla \times \mathcal{S}_{\Gamma_R} \mathbf{M}_R. \quad (2.11)$$

Here, Γ_R is the reflection of the bump Γ across the x_1x_2 -plane. If at a point $\mathbf{x} = (a, b, c) \in \Gamma$, the magnetic current \mathbf{M} is given by $\mathbf{M}(\mathbf{x}) = (m_1, m_2, m_3)$, then its image point on Γ_R is $\mathbf{x}' = (a, b, -c)$ and the image current is defined as $\mathbf{M}_R(\mathbf{x}') = (m_1, m_2, -m_3)$. It is straightforward to verify from (2.10) that $\mathbf{n} \times \mathbf{E}^{\text{sc}} = \mathbf{0}$ away from the bump (i.e., wherever $\mathbf{n} = (0, 0, 1)$). From standard jump condition relations, taking the limit of (2.10) to the boundary, it remains only to solve the boundary integral equation for \mathbf{M} :

$$\frac{1}{2} \mathbf{M} + \mathbf{n} \times \nabla \times \mathcal{S}_\Gamma \mathbf{M} + \mathbf{n} \times \nabla \times \mathcal{S}_{\Gamma_R} \mathbf{M}_R = -\mathbf{n} \times \mathbf{E}^{\text{inc}}$$

on Γ , where the integral operators are understood in their principal value sense. This is a second-kind (although not resonance-free) integral equation for a smooth bump.

2.2 The cavity case

Unfortunately, in the case of cavity deviations from a half-space, a more complicated representation is required. In order to make use of the method of images, following the approach of [29], we introduce an artificial boundary C_1 that covers the cavity, as shown in Fig. 1. The boundary C_1 must be sufficiently large so that its reflection C_2 across the x_1x_2 -plane does not intersect the cavity. The domain $\mathbb{R}^{3+} \cup \Omega_1$ is now decomposed into two sub-domains.

Definition 1. *In a slight abuse of notation, we will continue to use Ω_1 to denote the interior domain, bounded by Γ , B and C_1 . We will refer to the upper half-space outside of Ω_1 as the exterior domain.*

In the remainder of this paper, we will denote by $(\mathbf{E}^{\text{int}}, \mathbf{H}^{\text{int}})$ and $(\mathbf{E}^{\text{ext}}, \mathbf{H}^{\text{ext}})$ the scattered fields in the interior and exterior domains, respectively. The exterior scattered field $(\mathbf{E}^{\text{ext}}, \mathbf{H}^{\text{ext}})$ must satisfy Maxwell's equations (2.1) in $\mathbb{R}^{3+} \setminus \Omega_1$, together with the boundary condition

$$\mathbf{n} \times \mathbf{E}^{\text{ext}} = \mathbf{0} \quad \text{on } \Gamma^c \quad (2.12)$$

and the interface (or transmission) conditions on C_1 :

$$\begin{aligned} \mathbf{n} \times \mathbf{E}^{\text{ext}} &= \mathbf{n} \times \mathbf{E}^{\text{int}}, \\ \mathbf{n} \times \mathbf{H}^{\text{ext}} &= \mathbf{n} \times \mathbf{H}^{\text{int}}. \end{aligned} \quad (2.13)$$

Remark 2. *Since the domain Ω_1 contains edges, the fields \mathbf{E}^{int} and \mathbf{H}^{int} in Ω_1 are defined in the Sobolev space*

$$H(\text{curl}, \Omega_1) = \{\mathbf{u} \in (L^2(\Omega_1))^3, \nabla \times \mathbf{u} \in (L^2(\Omega_1))^3\},$$

where $(L^2(\Omega_1))^3$ denotes the space of component-wise square-integrable vector fields in Ω_1 . Moreover, the resulting integral equations we will derive are consisted by Fredholm operators of index zero in the trace space of $H(\text{curl}, \Omega_1)$, for which the Fredholm alternative still applies, i.e. uniqueness implies existence. We will omit the proof but refer the reader to [12, 27] for a detailed discussion.

As in the case of the bump, above, we can ensure that (2.12) is satisfied using the method of images. In particular, we now represent the exterior fields by

$$\begin{aligned} \mathbf{E}^{\text{ext}} &= -\frac{1}{ik} \nabla \times \nabla \times \mathcal{S}_{C_1}^H \mathbf{J} + \nabla \times \mathcal{S}_{C_1}^H \mathbf{M} + \nabla \times \mathcal{S}_B \mathbf{M}, \\ \mathbf{H}^{\text{ext}} &= \frac{1}{ik} \nabla \times \mathbf{E}^{\text{ext}} \\ &= \nabla \times \mathcal{S}_{C_1}^H \mathbf{J} + \frac{1}{ik} \nabla \times \nabla \times \mathcal{S}_{C_1}^H \mathbf{M} + \frac{1}{ik} \nabla \times \nabla \times \mathcal{S}_B \mathbf{M}, \end{aligned} \quad (2.14)$$

where image fields are given by

$$\begin{aligned} \nabla \times \nabla \times \mathcal{S}_{C_1}^H \mathbf{J} &= \nabla \times \nabla \times \mathcal{S}_{C_1} \mathbf{J} + \nabla \times \nabla \times \mathcal{S}_{C_2} \mathbf{J}_R, \\ \nabla \times \mathcal{S}_{C_1}^H \mathbf{M} &= \nabla \times \mathcal{S}_{C_1} \mathbf{M} + \nabla \times \mathcal{S}_{C_2} \mathbf{M}_R. \end{aligned} \quad (2.15)$$

The surface currents \mathbf{J}_R and \mathbf{M}_R on C_2 are the images of the currents \mathbf{J} and \mathbf{M} on C_1 . More specifically,

given $\mathbf{x} = (x, y, z) \in C_1$ and its image point $\mathbf{x}' = (x, y, -z) \in C_2$, the image currents are defined by

$$\begin{aligned} \mathbf{J}(\mathbf{x}') &= (-j_1, -j_2, j_3) & \text{if } \mathbf{J}(\mathbf{x}) &= (j_1, j_2, j_3), \\ \mathbf{M}(\mathbf{x}') &= (m_1, m_2, -m_3) & \text{if } \mathbf{M}(\mathbf{x}) &= (m_1, m_2, m_3). \end{aligned} \quad (2.16)$$

It is straightforward to verify that (2.12) is enforced by symmetry. Note that the last term in the electric field representation in (2.14) does not involve an image current. However, observe that B is part of the half-space boundary. It is easy to check that for any point beyond C_1 , sources defined on B make no contribution to the tangential electric field on Γ^c .

Remark 3. *We have introduced a magnetic current on B even though B is not part of the boundary of the exterior domain. This representation leads to a cancellation of hypersingular terms in the integral equation at the triple-junction where C_1 , C_2 , and B intersect, and hence to a bounded integral operator. This technique, which includes layer potentials on extra boundary components to alter the kernels in the integral equation is sometimes called the global density technique. For a more detailed discussion, see [20, 21, 29].*

For the interior scattered fields, we let

$$\begin{aligned} \mathbf{E}^{\text{int}} &= -\frac{1}{ik} \nabla \times \nabla \times \mathcal{S}_{C_1}^H \mathbf{J} + \nabla \times \mathcal{S}_{C_1}^H \mathbf{M} + \nabla \times \mathcal{S}_{B \cup \Gamma} \mathbf{M}, \\ \mathbf{H}^{\text{int}} &= \frac{1}{ik} \nabla \times \mathbf{E}^{\text{int}} \\ &= \nabla \times \mathcal{S}_{C_1}^H \mathbf{J} + \frac{1}{ik} \nabla \times \nabla \times \mathcal{S}_{C_1}^H \mathbf{M} + \frac{1}{ik} \nabla \times \nabla \times \mathcal{S}_{B \cup \Gamma} \mathbf{M}. \end{aligned} \quad (2.17)$$

Note that the only difference in the interior representation when compared with the exterior representation is that we have included a contribution from a magnetic current on the cavity Γ . Although C_2 , the image surface of C_1 , is not part of the boundary of Ω_1 , its contribution is added to the interior scattered fields by the similar reason as in Remark 3.

For convenience, given two surfaces Γ_s and Γ_t , and the current \mathbf{J} on Γ_s , we define the following two surface vector potentials for $\mathbf{x} \in \Gamma_t$ by

$$\mathcal{K}_{\Gamma_t, \Gamma_s} \mathbf{J}(\mathbf{x}) = \mathbf{n}(\mathbf{x}) \times \frac{1}{ik} \nabla \times \nabla \times \mathcal{S}_{\Gamma_s} \mathbf{J}(\mathbf{x}), \quad (2.18)$$

$$\mathcal{N}_{\Gamma_t, \Gamma_s} \mathbf{J}(\mathbf{x}) = \mathbf{n}(\mathbf{x}) \times \nabla \times \mathcal{S}_{\Gamma_s} \mathbf{J}(\mathbf{x}). \quad (2.19)$$

When Γ_s has a reflection, we define $\mathcal{K}_{\Gamma_t, \Gamma_s}^H \mathbf{J}$ and $\mathcal{N}_{\Gamma_t, \Gamma_s}^H \mathbf{J}$ to include the contribution from the reflected image currents as well, as in (2.15).

When $\Gamma_t = \Gamma_s = \Gamma$, the integral operators \mathcal{K} and \mathcal{N} become singular. More precisely, the integral in $\mathcal{K}_{\Gamma, \Gamma}$ is hypersingular and defined in the Hadamard principal-value sense, while $\mathcal{N}_{\Gamma, \Gamma}$ is defined in the Cauchy principal-value sense [15]. In this case, the following jump relations hold:

$$\lim_{\mathbf{x} \rightarrow \Gamma^\pm} \mathbf{n}(\mathbf{x}) \times \frac{1}{ik} \nabla \times \nabla \times \mathcal{S}_\Gamma \mathbf{J}(\mathbf{x}) = \mathcal{K}_{\Gamma, \Gamma} \mathbf{J}(\mathbf{x}), \quad (2.20)$$

$$\lim_{\mathbf{x} \rightarrow \Gamma^\pm} \mathbf{n}(\mathbf{x}) \times \nabla \times \mathcal{S}_\Gamma \mathbf{J}(\mathbf{x}) = \frac{1}{2} \mathbf{J}(\mathbf{x}) \pm \mathcal{N}_{\Gamma, \Gamma} \mathbf{J}(\mathbf{x}), \quad (2.21)$$

where Γ^\pm denotes the side that corresponds to the outward (+) or inward (−) normal, respectively.

Using the previous integral representations for the interior and exterior fields, the boundary value problem

$$\begin{aligned}
\nabla \times \mathbf{E} - ik\mathbf{H} &= 0, & \text{in } \Omega_1 \cup \mathbb{R}^{3+}, \\
\nabla \times \mathbf{H} + ik\mathbf{E} &= 0, & \text{in } \Omega_1 \cup \mathbb{R}^{3+}, \\
\mathbf{n} \times \mathbf{E}^{\text{ext}} &= \mathbf{n} \times \mathbf{E}^{\text{int}}, & \text{on } C_1, \\
\mathbf{n} \times \mathbf{H}^{\text{ext}} &= \mathbf{n} \times \mathbf{H}^{\text{int}}, & \text{on } C_1, \\
\mathbf{n} \times \mathbf{E}^{\text{int}} &= -\mathbf{n} \times \mathbf{E}^{\text{inc}} & \text{on } B \cup \Gamma,
\end{aligned} \tag{2.22}$$

along with jump conditions (2.20) and (2.21), immediately yields a system of integral equations for \mathbf{J} and \mathbf{M} :

$$\begin{aligned}
\mathbf{M} - \mathcal{N}_{C_1, \Gamma} \mathbf{M} &= \mathbf{0} & \text{on } C_1, \\
\mathbf{J} - \mathcal{K}_{C_1, \Gamma} \mathbf{M} &= \mathbf{0} & \text{on } C_1, \\
\frac{1}{2} \mathbf{M} + \mathcal{N}_{B, \Gamma} \mathbf{M} &= \mathbf{0} & \text{on } B, \\
\frac{1}{2} \mathbf{M} - \mathcal{K}_{\Gamma, C_1}^H \mathbf{J} + \mathcal{N}_{\Gamma, C_1}^H \mathbf{M} + \mathcal{N}_{\Gamma, B \cup \Gamma} \mathbf{M} &= -\mathbf{n} \times \mathbf{E}^{\text{inc}} & \text{on } \Gamma.
\end{aligned} \tag{2.23}$$

Due to the existence of corners, the integral system (2.23) is not second kind Fredholm equation. Nevertheless, the system is well conditioned once the corner singularity is well resolved numerically.

Remark 4. *Given the magnetic current \mathbf{M} along Γ , the first three equations the system (2.23) are explicitly solvable because they only involve the application of an off-surface layer potential. Therefore, our formulation can be reduced to an unknown magnetic current \mathbf{M} along Γ only. In particular, by substitution of the first three equations in (2.23) into the fourth equation in (2.23), we have the integral equation*

$$\frac{1}{2} \mathbf{M} - \mathcal{K}_{\Gamma, C_1}^H \mathcal{K}_{C_1, \Gamma} \mathbf{M} + \mathcal{N}_{\Gamma, C_1}^H \mathcal{N}_{C_1, \Gamma} \mathbf{M} - 2\mathcal{N}_{\Gamma, B} \mathcal{N}_{B, \Gamma} \mathbf{M} + \mathcal{N}_{\Gamma, \Gamma} \mathbf{M} = -\mathbf{n} \times \mathbf{E}^{\text{inc}} \tag{2.24}$$

for \mathbf{M} along Γ . Not only does this observation reduce the number of unknowns significantly, it will play a key role in avoiding low-frequency breakdown in the electric field, as shown in Section 4.

3 Existence and uniqueness

Since the integral system (2.23) consists of Fredholm operators of index zero, by the Fredholm alternative, existence follows from uniqueness. This is given by the following theorem.

Theorem 3.1. *Equation (2.23) admits a unique solution \mathbf{J} and \mathbf{M} for $k > 0$.*

Proof. It suffices to show that the system (2.23) has only the trivial solution for $k > 0$. For this, let us denote by Ω_2 the region bounded by C_2 , Γ and B . The proof involves three steps.

First, for \mathbf{J} and \mathbf{M} given in (2.23), define the induced electromagnetic field (\mathbf{E}, \mathbf{H}) for $\mathbf{x} \in \mathbb{R}^3 \setminus (\Omega_1 \cup \Omega_2)$ by

$$\begin{aligned}
\mathbf{E} &= -\frac{1}{ik} \nabla \times \nabla \times \mathcal{S}_{C_1}^H \mathbf{J} + \nabla \times \mathcal{S}_{C_1}^H \mathbf{M} + \nabla \times \mathcal{S}_B \mathbf{M}, \\
\mathbf{H} &= \nabla \times \mathcal{S}_{C_1}^H \mathbf{J} + \frac{1}{ik} \nabla \times \nabla \times \mathcal{S}_{C_1}^H \mathbf{M} + \frac{1}{ik} \nabla \times \nabla \times \mathcal{S}_B \mathbf{M},
\end{aligned} \tag{3.1}$$

and for $\mathbf{x} \in \Omega_1 \cup \Omega_2$,

$$\begin{aligned}\mathbf{E} &= -\frac{1}{ik} \nabla \times \nabla \times \mathcal{S}_{C_1}^H \mathbf{J} + \nabla \times \mathcal{S}_{C_1}^H \mathbf{M} + \nabla \times \mathcal{S}_{B \cup \Gamma} \mathbf{M}, \\ \mathbf{H} &= \nabla \times \mathcal{S}_{C_1}^H \mathbf{J} + \frac{1}{ik} \nabla \times \nabla \times \mathcal{S}_{C_1}^H \mathbf{M} + \frac{1}{ik} \nabla \times \nabla \times \mathcal{S}_{B \cup \Gamma} \mathbf{M}.\end{aligned}\tag{3.2}$$

From (2.23), we have that

$$\lim_{\substack{\mathbf{x} \rightarrow \Gamma^c \\ \mathbf{x} \in \mathbb{R}^3 \setminus (\Omega_1 \cup \Omega_2)}} \mathbf{n} \times \mathbf{E} = 0, \quad \lim_{\substack{\mathbf{x} \rightarrow B \cup \Gamma \\ \mathbf{x} \in \Omega_1}} \mathbf{n} \times \mathbf{E} = 0\tag{3.3}$$

and

$$[\mathbf{n} \times \mathbf{E}] = 0, \quad [\mathbf{n} \times \mathbf{H}] = 0 \quad \text{on } C_1,\tag{3.4}$$

where $[\cdot]$ denotes the jump in the corresponding the field.

Let $D \subset \mathbb{R}^{3+}$ be a finite region that is bounded by a sufficiently large hemisphere ∂D and the surfaces Γ^c and C_1 . Applying Green's first vector identity [15] to \mathbf{E} and its complex conjugate $\bar{\mathbf{E}}$ in D , and recalling the fact that $\nabla \cdot \mathbf{E} = 0$ in this region yields

$$\int_{\partial D \cup C_1} (\mathbf{n} \times \mathbf{E}) \cdot (\nabla \times \bar{\mathbf{E}}) dA = \iint_D (|\nabla \times \mathbf{E}|^2 - k^2 |\mathbf{E}|^2) dV.\tag{3.5}$$

Similarly, applying the same identity to \mathbf{E} in Ω_1 , we have

$$\int_{C_1 \cup \Gamma} (\mathbf{n} \times \mathbf{E}) \cdot (\nabla \times \bar{\mathbf{E}}) dA = \iint_{\Omega_1} (|\nabla \times \mathbf{E}|^2 - k^2 |\mathbf{E}|^2) dV.\tag{3.6}$$

Note that \mathbf{n} in (3.5) and (3.6) denotes the exterior normal with respect to the regions D and Ω_1 , and that the right hand side of both relations is purely real (for real k). Combining (3.5) and (3.6), using the continuity condition (3.4) along C_1 , and taking imaginary parts we have

$$\Im \int_{\partial D} (\mathbf{n} \times \mathbf{E}) \cdot (\nabla \times \bar{\mathbf{E}}) = \Im \int_{\Gamma} (\mathbf{n} \times \mathbf{E}) \cdot (\nabla \times \bar{\mathbf{E}}) = 0,\tag{3.7}$$

where \Im denotes the imaginary part. Lastly, since $\mathbf{n} \times \mathbf{E} = 0$ on Γ , relation (3.7) implies that the electric field is identically zero in D by Rellich's lemma [15]. By analytic continuation from C_1 into Ω_1 , we also obtain $\mathbf{E} = 0$ and $\mathbf{H} = 0$ in Ω_1 .

The second step in the proof is to show that the fields (\mathbf{E}, \mathbf{H}) in Ω_2 satisfy the following boundary conditions

$$\begin{aligned}\mathbf{n} \times \mathbf{E} &= \mathbf{M} && \text{on } \Gamma \cup B, \\ \mathbf{n} \times \mathbf{H} &= \mathbf{0} && \text{on } \Gamma \cup B, \\ \mathbf{n} \times \mathbf{E} &= \mathcal{N}_{C_2, \Gamma'} \mathbf{M} + \mathcal{N}_{C_2, \Gamma} \mathbf{M} && \text{on } C_2, \\ \mathbf{n} \times \mathbf{H} &= \mathcal{K}_{C_2, \Gamma'} \mathbf{M} + \mathcal{K}_{C_2, \Gamma} \mathbf{M} && \text{on } C_2.\end{aligned}\tag{3.8}$$

Here, just to clarify, \mathbf{n} on $\Gamma \cup B$ is the exterior normal with respect to Ω_1 and \mathbf{n} on C_2 is the exterior normal with respect to Ω_2 . The surface Γ' is the image of Γ with respect to the $x_1 x_2$ -plane, and \mathbf{M} on

Γ' is the corresponding image magnetic current. By (3.1), (3.2), and the jump relations (2.20), (2.21), we have that

$$[\mathbf{n} \times \mathbf{E}] = -\mathbf{M} \quad \text{and} \quad [\mathbf{n} \times \mathbf{H}] = 0 \quad \text{on } \Gamma \cup B. \quad (3.9)$$

Using the fact that $\mathbf{E} = \mathbf{0}$ and $\mathbf{H} = \mathbf{0}$ in Ω_1 , we obtain the desired boundary conditions (3.8) on $\Gamma \cup B$ for the fields (\mathbf{E}, \mathbf{H}) in Ω_2 .

Turning to the boundary C_2 , we have the jump conditions

$$[\mathbf{n} \times \mathbf{E}] = -\mathbf{M}' + \mathcal{N}_{C_2, \Gamma} \mathbf{M} \quad \text{and} \quad [\mathbf{n} \times \mathbf{H}] = -\mathbf{J}' + \mathcal{K}_{C_2, \Gamma} \mathbf{M} \quad \text{on } C_2. \quad (3.10)$$

Here, \mathbf{J}' and \mathbf{M}' are the image surface currents on C_2 . By equation (2.23) and symmetry,

$$\mathbf{M}' = \mathcal{N}_{C_2, \Gamma'} \mathbf{M}' \quad \text{and} \quad \mathbf{J}' = \mathcal{K}_{C_2, \Gamma'} \mathbf{M}' \quad \text{on } C_2, \quad (3.11)$$

where \mathbf{M}' on Γ' is again the image magnetic current of \mathbf{M} on Γ . Combining (3.10) and (3.11), we obtain the remaining boundary conditions in (3.8).

The third, and final, step in the proof is to show that the electromagnetic field satisfying (3.8) is identically zero. For this, extend \mathbf{E} and \mathbf{H} from Ω_2 to $\mathbb{R}^{3-} \setminus \Omega_2$ by letting

$$\begin{aligned} \mathbf{E} &= -\nabla \times \mathcal{S}_{\Gamma'} \mathbf{M}' + \nabla \times \mathcal{S}_{\Gamma} \mathbf{M} \\ \mathbf{H} &= -\frac{1}{ik} \nabla \times \nabla \times \mathcal{S}_{\Gamma'} \mathbf{M}' + \frac{1}{ik} \nabla \times \nabla \times \mathcal{S}_{\Gamma} \mathbf{M}. \end{aligned} \quad (3.12)$$

It is easy to see that (\mathbf{E}, \mathbf{H}) is an electromagnetic field satisfying

$$\mathbf{n} \times \mathbf{H} = \mathbf{0} \quad \text{on } \Gamma^c. \quad (3.13)$$

Following the same argument as in the first step (with \mathbf{E} and \mathbf{H} exchanged), we must have $\mathbf{E} = \mathbf{0}$ and $\mathbf{H} = \mathbf{0}$ in Ω_2 , which implies $\mathbf{M} = \mathbf{0}$ on Γ . Therefore, by (2.23), we obtain $\mathbf{J} = \mathbf{0}$ and $\mathbf{M} = \mathbf{0}$ on C_1 . \square

A similar proof can be obtained in the case where $\Re(k) > 0$ and $\Im(k) > 0$. In the static case where $k = 0$, our representation is not valid and must be altered. However, the existence and uniqueness can be handled directly by electro- and magneto-static arguments.

4 Low-frequency breakdown

It is clear that the integral representations (2.14) and (2.17) are numerically unstable as $k \rightarrow 0$ due to the explicit $1/ik$ scaling. This problem is not intrinsic to the Maxwell system (2.1), where the electric and magnetic field simply uncouple in the static limit. Rather, it is due to the use of vector currents \mathbf{J}, \mathbf{M} as the unknowns. The resulting loss of precision is generally referred to as *low-frequency breakdown* [40]. Rather than develop a new mathematical formalism to overcome this, as in [16, 17], we modify our method described above to create a representation that is stable as $k \rightarrow 0$. In short, using properties of the electromagnetic fields and vector identities, we are able to express the

electric field only in terms of \mathbf{M} , and in the process, eliminate the terms which scale as $1/ik$. The magnetic field representation still formally suffers from low-frequency breakdown, but numerically it is relatively benign as $k \rightarrow 0$.

In order to express \mathbf{E} only in terms of well-scaled operators of \mathbf{M} , we require the following identity.

Lemma 4.1. *Let Γ be an open surface with smooth boundary ℓ , and let \mathbf{J} be a smooth tangential vector field along Γ . Then*

$$\frac{1}{ik} \nabla \times \nabla \times \mathcal{S}_\Gamma \mathbf{J} = -ik \mathcal{S}_\Gamma \mathbf{J} + \nabla \mathcal{S}_\Gamma \left(\frac{\nabla_\Gamma \cdot \mathbf{J}}{ik} \right) - \nabla \mathcal{S}_\ell \left(\frac{\mathbf{J} \cdot \mathbf{b}}{ik} \right) \quad (4.1)$$

where $\mathbf{b} = \boldsymbol{\tau} \times \mathbf{n}$ is the outward bi-normal vector along ℓ , with $\boldsymbol{\tau}$ the unit tangent vector along ℓ and \mathbf{n} the surface normal (oriented so that \mathbf{b} points away from the surface).

Proof. Using the point-wise vector identity $\nabla \times \nabla \times \mathbf{a} = -\Delta \mathbf{a} + \nabla \nabla \cdot \mathbf{a}$, we have

$$\frac{1}{ik} \nabla \times \nabla \times \mathcal{S}_\Gamma \mathbf{J} = -\frac{1}{ik} \Delta \mathcal{S}_\Gamma \mathbf{J} + \nabla \nabla \cdot \mathcal{S}_\Gamma \left(\frac{\mathbf{J}}{ik} \right). \quad (4.2)$$

Since $\mathcal{S}_\Gamma \mathbf{J}$ is a vector-valued Helmholtz potential, it is clear that

$$-\frac{1}{ik} \Delta \mathcal{S}_\Gamma \mathbf{J} = -ik \mathcal{S}_\Gamma \mathbf{J}. \quad (4.3)$$

For the second term on the right-hand side of (4.2), we apply Stokes's identity [35] on the surface Γ :

$$\begin{aligned} \nabla \cdot \mathcal{S}_\Gamma \left(\frac{\mathbf{J}}{ik} \right) &= - \int_\Gamma \nabla_{\mathbf{y}, \Gamma} \cdot \left(G(\mathbf{x}, \mathbf{y}) \frac{\mathbf{J}(\mathbf{y})}{ik} \right) dA_y + \int_\Gamma G(\mathbf{x}, \mathbf{y}) \frac{\nabla_\Gamma \cdot \mathbf{J}(\mathbf{y})}{ik} dA_y \\ &= -\mathcal{S}_\ell \left(\frac{\mathbf{J} \cdot \mathbf{b}}{ik} \right) + \mathcal{S}_\Gamma \left(\frac{\nabla_\Gamma \cdot \mathbf{J}}{ik} \right), \end{aligned} \quad (4.4)$$

where $\nabla_{\mathbf{y}, \Gamma} \cdot$ denotes the surface divergence with respect to the variable \mathbf{y} . □

Corollary 4.2. *Let Γ be a surface whose boundary ℓ is a curve that lies on the plane $x_3 = 0$, and let \mathbf{J} and \mathbf{M} be surface electric and magnetic currents on Γ with image currents defined in (2.16). Note that the image currents also lie along $x_3 = 0$. Then*

$$\begin{aligned} \frac{1}{ik} \nabla \times \nabla \times \mathcal{S}_\Gamma^H \mathbf{J} &= -ik \mathcal{S}_\Gamma^H \mathbf{J} + \nabla \mathcal{S}_\Gamma^H \left(\frac{\nabla_\Gamma \cdot \mathbf{J}}{ik} \right), \\ \frac{1}{ik} \nabla \times \nabla \times \mathcal{S}_\Gamma^H \mathbf{M} &= -ik \mathcal{S}_\Gamma^H \mathbf{M} + \nabla \mathcal{S}_\Gamma^H \left(\frac{\nabla_\Gamma \cdot \mathbf{M}}{ik} \right) - 2 \nabla \mathcal{S}_\ell \left(\frac{\mathbf{M} \cdot \mathbf{b}}{ik} \right). \end{aligned} \quad (4.5)$$

We can now establish the following identity:

Lemma 4.3. *For a tangential electric and magnetic currents \mathbf{J} , \mathbf{M} along Γ , defined as in (2.17),*

$$\frac{\nabla_{C_1} \cdot \mathbf{J}}{ik} = -\mathbf{n} \cdot \nabla \times \mathcal{S}_\Gamma \mathbf{M}. \quad (4.6)$$

Proof. First, apply Corollary 4.2 to rewrite the representation of the electric field in the form

$$\begin{aligned}\mathbf{E}^{\text{ext}} &= ik\mathcal{S}_{C_1}^H \mathbf{J} - \nabla \mathcal{S}_{C_1}^H \left(\frac{\nabla_{C_1} \cdot \mathbf{J}}{ik} \right) + \nabla \times \mathcal{S}_{C_1}^H \mathbf{M} + \nabla \times \mathcal{S}_B \mathbf{M}, \\ \mathbf{E}^{\text{int}} &= ik\mathcal{S}_{C_1}^H \mathbf{J} - \nabla \mathcal{S}_{C_1}^H \left(\frac{\nabla_{C_1} \cdot \mathbf{J}}{ik} \right) + \nabla \times \mathcal{S}_{C_1}^H \mathbf{M} + \nabla \times \mathcal{S}_{B \cup \Gamma} \mathbf{M}.\end{aligned}\tag{4.7}$$

Taking the difference of \mathbf{E}^{ext} and \mathbf{E}^{int} in (4.7), computing normal components, using the jump relations for the single layer potential, and recalling the continuity condition

$$\mathbf{n} \cdot \mathbf{E}^{\text{ext}} = \mathbf{n} \cdot \mathbf{E}^{\text{int}} \quad \text{on } C_1,\tag{4.8}$$

yields the desired result in (4.6). \square

We can now derive low-frequency versions of integral equation (2.24) and representations for the electric and magnetic fields.

4.1 A modified integral equation

Using the previous results, we can now derive an integral equation along Γ which does not suffer from low-frequency breakdown, as does equation (2.24). Inspection of the various terms in (2.24) shows that $1/ik$ scaling is present only in the term

$$- \mathcal{K}_{\Gamma, C_1}^H \mathcal{K}_{C_1, \Gamma} \mathbf{M}.\tag{4.9}$$

By application of Lemma 4.1 and use of the result in Corollary 4.2, this term can be replaced as

$$- \mathcal{K}_{\Gamma, C_1}^H \mathcal{K}_{C_1, \Gamma} \mathbf{M} = \mathbf{n} \times ik\mathcal{S}_{C_1}^H \mathbf{J} - \mathbf{n} \times \nabla \mathcal{S}_{C_1}^H \left(\frac{\nabla_{C_1} \cdot \mathbf{J}}{ik} \right),\tag{4.10}$$

where, recalling that by equation (2.23)

$$\mathbf{J} = \mathcal{K}_{C_1, \Gamma} \mathbf{M} = \mathbf{n} \times \left(\frac{1}{ik} \nabla \times \nabla \times \mathcal{S}_{\Gamma} \mathbf{M} \right).\tag{4.11}$$

Using (4.11), the first term in (4.10) can be rewritten in terms of \mathbf{M} on Γ :

$$\mathbf{n} \times ik\mathcal{S}_{C_1}^H \mathbf{J} = \mathbf{n} \times \mathcal{S}_{C_1}^H (\mathbf{n} \times \nabla \times \nabla \times \mathcal{S}_{\Gamma} \mathbf{M}).\tag{4.12}$$

Combining (4.12) and (4.6), we can have the modified equation along Γ :

$$\begin{aligned}\frac{1}{2} \mathbf{M} + \mathbf{n} \times \mathcal{S}_{C_1}^H (\mathbf{n} \times \nabla \times \nabla \times \mathcal{S}_{\Gamma} \mathbf{M}) + \mathbf{n} \times \nabla \mathcal{S}_{C_1}^H (\mathbf{n} \cdot \nabla \times \mathcal{S}_{\Gamma} \mathbf{M}) \\ + \mathcal{N}_{\Gamma, C_1}^H \mathcal{N}_{C_1, \Gamma} \mathbf{M} - 2\mathcal{N}_{\Gamma, B} \mathcal{N}_{B, \Gamma} \mathbf{M} + \mathcal{N}_{\Gamma, \Gamma} \mathbf{M} = -\mathbf{n} \times \mathbf{E}^{\text{inc}}.\end{aligned}\tag{4.13}$$

This is equivalent to (2.24), but is clearly immune from low-frequency breakdown.

4.2 Field calculations

Furthermore, given the solution \mathbf{M} to integral equation (4.13), we have the following representations for the electric field which do not suffer from low-frequency breakdown:

$$\begin{aligned}\mathbf{E}^{\text{ext}} &= ik\mathcal{S}_{C_1}^H \mathcal{K}_{C_1, \Gamma} \mathbf{M} - \nabla \mathcal{S}_{C_1}^H (\mathbf{n} \cdot \nabla \times \mathcal{S}_\Gamma \mathbf{M}) + \nabla \times \mathcal{S}_{C_1}^H \mathbf{M} + \nabla \times \mathcal{S}_B \mathbf{M}, \\ \mathbf{E}^{\text{int}} &= ik\mathcal{S}_{C_1}^H \mathcal{K}_{C_1, \Gamma} \mathbf{M} - \nabla \mathcal{S}_{C_1}^H (\mathbf{n} \cdot \nabla \times \mathcal{S}_\Gamma \mathbf{M}) + \nabla \times \mathcal{S}_{C_1}^H \mathbf{M} + \nabla \times \mathcal{S}_{B \cup \Gamma} \mathbf{M}.\end{aligned}\quad (4.14)$$

Once \mathbf{M} along Γ has been obtained by solving (4.13), we can obtain \mathbf{M} on $C_1 \cup B$ through (2.23). Evaluation via representation (4.14) is stable as $k \rightarrow 0$. On the other hand, we are left with computing the magnetic field as

$$\mathbf{H}^{\text{ext}} = \frac{1}{ik} \nabla \times \mathbf{E}^{\text{ext}}, \quad \mathbf{H}^{\text{int}} = \frac{1}{ik} \nabla \times \mathbf{E}^{\text{int}}, \quad (4.15)$$

which are inherently first-order operations in the variable \mathbf{M} and will obviously suffer from low-frequency breakdown. As an alternative, we may try to rewrite \mathbf{H} using vector identities and in terms of the variable \mathbf{J} . In the case of \mathbf{H}^{int} , for example, we have

$$\mathbf{H}^{\text{int}} = \nabla \times \mathcal{S}_{C_1}^H \mathbf{J} + \frac{1}{ik} \nabla \times \nabla \times \mathcal{S}_{C_1}^H \mathbf{M} + \frac{1}{ik} \nabla \times \nabla \times \mathcal{S}_{B \cup \Gamma} \mathbf{M}. \quad (4.16)$$

The expression for \mathbf{H}^{ext} is nearly identical. Any attempt using the previous lemmas or corollary to simplify this representation will require the (numerical) evaluation of the quantities \mathbf{J} , $\nabla_\Gamma \cdot \mathbf{M}/ik$, and $\mathbf{M} \cdot \mathbf{b}/ik$. Empirically, these expressions can be evaluated at the cost of a mild loss of numerical precision. The quantity \mathbf{J} can be directly evaluated via $\mathbf{J} = \mathcal{K}_{C_1, \Gamma} \mathbf{M}$, or by using the identity:

$$\mathbf{J} = \mathbf{n} \times \left(-ik\mathcal{S}_\Gamma \mathbf{M} + \nabla \mathcal{S}_\Gamma \left(\frac{\nabla_\Gamma \cdot \mathbf{M}}{ik} \right) - \nabla \mathcal{S}_\ell \left(\frac{\mathbf{M} \cdot \mathbf{b}}{ik} \right) \right). \quad (4.17)$$

We compute the function $\rho_M = \nabla_\Gamma \cdot \mathbf{M}/ik$ merely by spectral differentiation in a 10th-order Legendre discretization, and the term $\phi_M = \mathbf{M} \cdot \mathbf{b}/ik$ by extrapolation.

These schemes lead to roughly an $\mathcal{O}(\log k)$ loss in absolute precision. For example, as discussed in the numerical examples section, for $k \approx 10^{-10}$, we are able to obtain approximately 6 digits of accuracy.

Remark 5. *The function ϕ_M cannot be evaluated naively for small k . Numerical experiments indicate that $\mathbf{M} \cdot \mathbf{b} \approx \mathcal{O}(k)$ as $k \rightarrow 0$, but we have not found a proof of this fact. Similar to ρ_M , we numerically found that ϕ_M has a low-frequency limit. In particular, we can formally expand:*

$$\frac{\mathbf{M} \cdot \mathbf{b}}{ik} = m_1 + km_2 + \dots \quad (4.18)$$

The quantity ϕ_M can then be evaluated for several distinct non-zero values of k , and the coefficients m_j can be estimated to the desired order of accuracy. These estimated values can then be used to compute ϕ_M for any $k \geq 0$. The result can then be used in (4.17) to evaluate the \mathbf{H} field. This form of low-frequency breakdown is, therefore, much less pernicious than that addressed by Lemma 4.3, and that present in the evaluation of ρ_M , which is sometimes referred to as dense-mesh breakdown. Nevertheless, we consider it to be an open problem

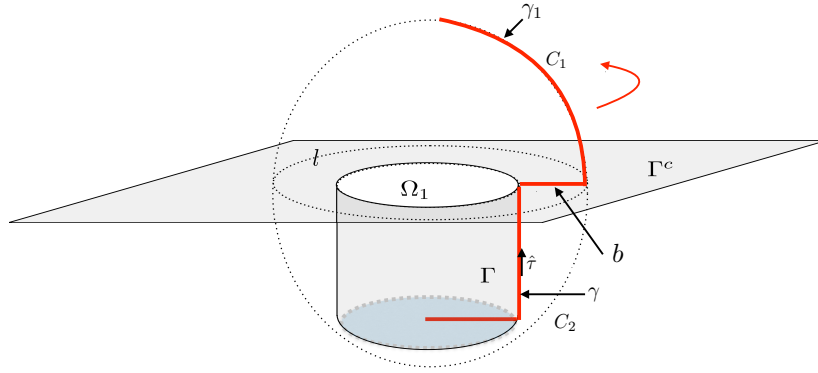


Figure 3: Axisymmetric cavity with generating curve $g = \gamma \cup b \cup \gamma_1$.

to find an integral formulation which avoids the need for this asymptotic approach.

5 Separation of variables for boundary integral operators

For arbitrarily shaped cavities, a full three-dimensional treatment of quadratures and geometry discretization is required to evaluate the integral operators discussed in the previous section, not to mention schemes to solve the corresponding integral equations. While fast multipole methods reduce the computational complexity of applying such integral operators to $\mathcal{O}(N)$ or $\mathcal{O}(N \log N)$, (see for example, [14]) and high-order quadratures have been developed for weakly-singular kernels on arbitrary surface triangulations [10], the associated constants implicit in the $\mathcal{O}(\cdot)$ scaling are relatively large. On the other hand, for a wide class of geometries – namely those with rotational symmetry – two useful accelerations are easily obtained. First, in problems for which the Green’s function is translation invariant, one can apply separation of variables in the azimuthal angle, θ , relative to the x_3 -axis, and then Fourier decompose the problem. This transforms the original integral equation, defined on a surface in three dimensions, into a sequence of uncoupled integral equations (one for each Fourier mode) defined along a one-dimensional *generating curve*. Second, the resulting linear systems are much smaller, and the associated quadrature issues are much easier to address [18, 23, 24, 34, 36, 39]. We avoid a detailed description of axisymmetric integral equation solvers here, and instead point the reader to the previous references for discussions related to quadrature and kernel evaluation. In what follows below, we provide a brief description of the discretization relevant to our cavity scattering problem.

5.1 Modal kernels and operators

A simple example of the geometrical setup is shown in Fig. 3. A point $\mathbf{x} = (x_1, x_2, x_3)$ in \mathbb{R}^3 will be denoted in the usual cylindrical coordinates as $\mathbf{x} = (r, \theta, z)$. The standard unit vectors in cylindrical coordinates will be denoted as $(\mathbf{e}_r, \mathbf{e}_\theta, \mathbf{e}_z)$. The generating curve is given by $g = \gamma \cup b \cup \gamma_1$, which we assume is parameterized by $g(s) = (r(s), z(s))$, where s denotes arclength. The tangent vector along the generating curve is then $\mathbf{t} = \frac{dr}{ds} \mathbf{e}_r + \frac{dz}{ds} \mathbf{e}_z$, and the exterior normal \mathbf{n} is given by $\mathbf{n} = \frac{dz}{ds} \mathbf{e}_r - \frac{dr}{ds} \mathbf{e}_z$.

Relative to the surface frame \mathbf{t} , \mathbf{n} , \mathbf{e}_θ , any tangential vector field \mathbf{J} along $\Gamma \cup B \cup C_1$ can be written as:

$$\mathbf{J}(s, \theta) = \sum_m (J_m^1(s) \mathbf{t} + J_m^2(s) \mathbf{e}_\theta) e^{im\theta}. \quad (5.1)$$

In the scalar case, a second-kind boundary integral equation on a body of revolution Ω ,

$$u(\mathbf{x}) + \int_{\partial\Omega_1} G(\mathbf{x} - \mathbf{x}') u(\mathbf{x}') dA(\mathbf{x}') = f(\mathbf{x}), \quad (5.2)$$

can immediately be decomposed into a sequence of decoupled equations

$$u_m(\mathbf{x}) + 2\pi \int_g G_m(r, z, r', z') u_m(r', z') r' ds(r', z') = f_m(r, z) \quad (5.3)$$

where

$$\begin{aligned} u(\mathbf{x}) &= \sum_m u_m(r, z) e^{im\theta}, \\ f(\mathbf{x}) &= \sum_m f_m(r, z) e^{im\theta}, \\ G(\mathbf{x} - \mathbf{x}') &= \sum_m G_m(r, z, r', z') e^{im(\theta - \theta')}. \end{aligned} \quad (5.4)$$

However, in the vector-valued integral equation setting, the components of the unknown \mathbf{J} do not fully separate when expressed in terms of local, tangential coordinates [36]. We therefore need to compute the action of the single-layer potential operator \mathcal{S} , and its derivatives, on a tangential density \mathbf{J} . Using the fact that relative to the Cartesian unit vectors \mathbf{e}_1 , \mathbf{e}_2 , \mathbf{e}_3 :

$$\begin{aligned} \mathbf{e}_r &= \cos \theta \mathbf{e}_1 + \sin \theta \mathbf{e}_2, \\ \mathbf{e}_\theta &= -\sin \theta \mathbf{e}_1 + \cos \theta \mathbf{e}_2, \\ \mathbf{e}_z &= \mathbf{e}_3, \end{aligned} \quad (5.5)$$

it is straightforward to verify that if \mathbf{J} is as in (5.1), then

$$\mathcal{S}_\Gamma \mathbf{J} = \sum_m (c_m^1 \mathbf{e}_r + c_m^2 \mathbf{e}_\theta + c_m^3 \mathbf{e}_z) e^{im\theta} \quad (5.6)$$

where

$$\begin{aligned} c_m^1 &= \int_\gamma G_m^{\cos}(r, z, r', z') J_m^1(s) \frac{dr'}{ds} r' ds - i \int_\gamma G_m^{\sin}(r, z, r', z') J_m^2(s) r' ds, \\ c_m^2 &= i \int_\gamma G_m^{\sin}(r, z, r', z') J_m^1(s) \frac{dr'}{ds} r' ds + \int_\gamma G_m^{\cos}(r, z, r', z') J_m^2(s) r' ds, \\ c_m^3 &= \int_\gamma G_m(r, z, r', z') J_m^1(s) \frac{dz'}{ds} r' ds, \end{aligned} \quad (5.7)$$

and the kernels G_m , G_m^{\cos} , and G_m^{\sin} are given by:

$$\begin{aligned} G_m(r, z, r', z') &= \frac{1}{2\pi} \int_0^{2\pi} \frac{e^{ikR}}{4\pi R} e^{-im\phi} d\phi, \\ G_m^{\cos}(r, z, r', z') &= \frac{1}{2\pi} \int_0^{2\pi} \frac{e^{ikR}}{4\pi R} \cos m\phi \cos \phi d\phi, \\ G_m^{\sin}(r, z, r', z') &= \frac{1}{2\pi} \int_0^{2\pi} \frac{e^{ikR}}{4\pi R} \sin m\phi \sin \phi d\phi, \end{aligned} \quad (5.8)$$

with R given by the Euclidian distance in cylindrical coordinates:

$$R = \sqrt{r^2 + r'^2 - 2rr' \cos \phi + (z - z')^2}, \quad (5.9)$$

with $\phi = \theta - \theta'$ denoting the azimuthal angle between \mathbf{x} and \mathbf{x}' . It is understood in the previous formulas that for *source* points (r', z') on the boundary, evaluation is in terms of the parameterization of the curve, i.e.: $r' = r(s')$ and $z' = z(s')$ for some s' . Expressions for all other boundary operators, for example \mathcal{K} and \mathcal{N} , can be obtained from the above expressions by taking derivatives with respect to sources and targets.

In particular, formulas for the curl and divergence of $\mathbf{S}\mathbf{J}$ can be calculated immediately from application of these operators in cylindrical coordinates to expression (5.6), with the partial derivatives being taken directly on the kernel functions. Differentiation with respect to θ is diagonal. For this reason, we omit these formulas here.

However, it is useful to provide an expression for a less common differential operator, namely $\nabla \nabla \cdot$, used when applying $\nabla \times \nabla \times$ to Helmholtz potentials, see Lemma 4.1. The operator \mathcal{K} involves this. To this end, we have:

$$\begin{aligned} \nabla \nabla \cdot \mathbf{S}\mathbf{J} &= \left(-\frac{c_m^1}{r^2} + \frac{1}{r} \frac{\partial c_m^1}{\partial r} + \frac{\partial^2 c_m^1}{\partial r^2} - \frac{im}{r^2} c_m^2 + \frac{im}{r} \frac{\partial c_m^2}{\partial r} + \frac{\partial^2 c_m^3}{\partial r \partial z} \right) \mathbf{e}_r \\ &\quad + \frac{im}{r} \left(\frac{c_m^1}{r} + \frac{\partial c_m^1}{\partial r} + \frac{im}{r} c_m^2 + \frac{\partial c_m^3}{\partial z} \right) \mathbf{e}_\theta + \left(\frac{1}{r} \frac{\partial c_m^1}{\partial z} + \frac{\partial^2 c_m^1}{\partial z \partial r} + \frac{im}{r} \frac{\partial c_m^2}{\partial z} + \frac{\partial^2 c_m^3}{\partial z^2} \right) \mathbf{e}_z. \end{aligned} \quad (5.10)$$

Furthermore, in order to discretize (4.13), the modified integral equation free from low-frequency breakdown, we also require the potential induced by a scalar density on Γ . In particular, in equation (4.13), the term $\mathbf{n} \cdot \nabla \times \mathbf{S}\mathbf{M}$ is a scalar function to which a layer potential operator must be applied. Using equation (5.3)-(5.4), the calculation of scalar single layer potential is straightforward. The gradient is then given using the standard form of the gradient in cylindrical coordinates.

Remark 6. While separation of variables has permitted us to reduce two dimensional surface integrals to one dimensional line integrals, the kernels G_m , G_m^{\cos} and G_m^{\sin} defined in (5.8) are not available in closed form. See [24] for a description on how to efficiently evaluate them. In the numerical examples of this work, we merely use adaptive Gaussian quadrature for their evaluation. Significant speedups in the resulting code could be obtained by optimizing their calculation. Our goal is merely to demonstrate the behavior of our novel integral equation for scattering from cavities.

5.2 Discretization

We discretize each smooth segment of the piecewise-smooth boundary by a set of panels of uniform length, so that there are at least 12 points per wavelength. We then refine the end panels on each segment dyadically until the smallest segment is of length ϵ , where ϵ is the desired precision. Each panel is discretized using 10 Gauss-Legendre nodes, and we utilize 10th-order accurate generalized Gaussian quadratures [11] as the basis for a Nyström method (which takes into account the logarithmic singularity in the kernel). For a review and comparison of various Nyström-type discretizations, see [22]. Adaptive Gaussian quadrature is used to compute the modal Green's function element by element, as well as for nearly-singular interactions.

In a slight abuse of notation, for an integral operator \mathcal{K} , we will denote by \mathbf{K}_m the matrix obtained from discretizing the m^{th} mode of \mathcal{K} . Using the formulas of the previous section, we can discretize equation (4.13) as:

$$\left(\frac{1}{2} \mathbf{I} + ik \mathbf{TS}_m^{(1)} \mathbf{K}_m + \mathbf{TS}_m^{(2)} \mathbf{US}_m^{(3)} + \mathbf{N}_m^{(2)} \mathbf{N}_m^{(1)} - 2\mathbf{N}_m^{(4)} \mathbf{N}_m^{(3)} + \mathbf{N}_m^{(5)} \right) \mathbf{M}_m = -\mathbf{TE}_m^{\text{inc}} \quad (5.11)$$

where the matrices above are discretizations of a *single mode* of the continuous operators as follows:

$$\begin{aligned} \mathbf{I} &= \mathcal{I}, & \mathbf{T} &= \mathbf{n} \times, & \mathbf{U} &= \mathbf{n} \cdot, \\ \mathbf{S}_m^{(1)} &\approx \mathcal{S}_{C_1, m'}^H, & \mathbf{S}_m^{(2)} &\approx \nabla \mathcal{S}_{C_1, m'}^H, & \mathbf{S}_m^{(3)} &\approx \nabla \times \mathcal{S}_{\Gamma, m'}, \\ \mathbf{K}_m &\approx \mathcal{K}_{C_1, \Gamma, m'}, & \mathbf{N}_m^{(1)} &\approx \mathcal{N}_{C_1, \Gamma, m'}, & \mathbf{N}_m^{(2)} &\approx \mathcal{N}_{\Gamma, C_1, m'}^H, \\ \mathbf{N}_m^{(3)} &\approx \mathcal{N}_{B, \Gamma, m'}, & \mathbf{N}_m^{(4)} &\approx \mathcal{N}_{\Gamma, B, m'}, & \mathbf{N}_m^{(5)} &\approx \mathcal{N}_{\Gamma, \Gamma, m'}, \end{aligned} \quad (5.12)$$

and the discretization of the m^{th} mode of the solution \mathbf{M} is given by \mathbf{M}_m and the incoming data \mathbf{E}^{inc} is given by $\mathbf{E}_m^{\text{inc}}$. The matrix $\mathbf{N}_m^{(5)}$ correspond to a layer potential with singular kernel, and is therefore obtained via discretization with generalized Gaussian quadrature. All other matrices correspond to layer potentials without singular kernels (no self-interactions) and therefore can be discretized using smooth and adaptive Gaussian quadrature (near geometric refinement). The matrix \mathbf{K}_m can be constructed by discretizing either the operator $\nabla \times \nabla \times \mathcal{S}$, or by invoking Lemma 4.1.

6 Numerical examples

In this section, we illustrate the performance of our algorithm for three distinct piecewise smooth cavity structures. Because of the singularities induced in the densities at the non-smooth junction points, dyadic refinement is applied on each segment, as discussed in section 5.2.

We normalize the physical length scale so that the cavity can be covered by a hemisphere C_1 with radius 2, centered at $(0, 0, 0)$. To test the accuracy of the solver, we first create an artificial problem, in which the exact solution is known. For this, we choose the field in $\mathbb{R}^{3+} \setminus \Omega_1$ to be generated by a current loop located in Ω_1 , and the field in Ω_1 to be generated by a current loop located in $\mathbb{R}^{3+} \setminus \Omega_1$.

In other words, the exact exterior field in $\mathbb{R}^{3+} \setminus \Omega_1$ is

$$\begin{aligned}\mathbf{E}_e^{\text{ext}} &= -\frac{1}{ik} \nabla \times \nabla \times S_{\ell_1}^H \mathbf{J}_\theta, \\ \mathbf{H}_e^{\text{ext}} &= \nabla \times S_{\ell_1}^H \mathbf{J}_\theta,\end{aligned}\tag{6.1}$$

and the exact interior field in Ω_1 is given by

$$\begin{aligned}\mathbf{E}_e^{\text{int}} &= -\frac{1}{ik} \nabla \times \nabla \times S_{\ell_2}^H \mathbf{J}_\theta, \\ \mathbf{H}_e^{\text{int}} &= \nabla \times S_{\ell_2}^H \mathbf{J}_\theta,\end{aligned}\tag{6.2}$$

where ℓ_1 and ℓ_2 are horizontal circular loops with radius 0.5. The loop ℓ_1 is located in Ω_1 and ℓ_2 in $\mathbb{R}^{3+} \setminus \Omega_1$, each with current density $\mathbf{J} = e^{i\theta} \mathbf{e}_\theta$. Given the field representation in (2.14) and (2.17), one can introduce the jump conditions along C_1 and the boundary condition on $B \cup \Gamma$ consistent with the specified analytic solution. Note that, although we only use a single azimuthal mode in the current that defines the exact solution, the number of Fourier modes needed to resolve the actual field depends on the location of the loops. To test only the solver for the $m = 1$ mode, we center ℓ_1 at $(0, 0, 0.3)$ and ℓ_2 at $(0, 0, 3.3)$. To test the full three-dimensional problem, we place the center of ℓ_1 at $(0, 0, 0.3)$ but move the second loop off-axis, centering ℓ_2 at $(1.2, 0, 3.3)$. We use as many modes as required in order to resolve the data to precision ϵ (which depends in part on the governing frequency k).

We also solve a true scattering problem with incident plane wave:

$$\begin{aligned}\mathbf{E}^{\text{inc}} &= (\hat{\mathbf{d}} \times \hat{\mathbf{p}}) \times \hat{\mathbf{d}} e^{ik\hat{\mathbf{d}} \cdot \mathbf{x}} - (\hat{\mathbf{d}}' \times \hat{\mathbf{p}}') \times \hat{\mathbf{d}}' e^{ik\hat{\mathbf{d}}' \cdot \mathbf{x}} \\ \mathbf{H}^{\text{inc}} &= \hat{\mathbf{d}} \times \hat{\mathbf{p}} e^{ik\hat{\mathbf{d}} \cdot \mathbf{x}} - \hat{\mathbf{d}}' \times \hat{\mathbf{p}}' e^{ik\hat{\mathbf{d}}' \cdot \mathbf{x}}\end{aligned}$$

where $\hat{\mathbf{d}}$ is the propagation direction, $\hat{\mathbf{p}}$ is the polarization, $\hat{\mathbf{d}}'$ and $\hat{\mathbf{p}}'$ are the reflected directions with respect to $x_3 = 0$. Through out all the examples, we choose

$$\begin{aligned}\hat{\mathbf{d}} &= (\cos(\pi/4) \sin(\pi/8), \sin(\pi/4) \sin(\pi/8), \cos(\pi/8)), \\ \hat{\mathbf{p}} &= (\cos(\pi/5) \sin(\pi/10), \sin(\pi/5) \sin(\pi/10), \cos(\pi/10)).\end{aligned}$$

We make use of the following notation in subsequent tables:

- k : the governing wavenumber,
- N_f : the number of Fourier modes used to resolve the solution,
- N_{pts} : the total number of points used to discretize Γ , C_1 and B ,
- N_{tot} : the total number of unknowns in the discretized integral equation,
- T_{matgen} : the time (secs.) to construct the relevant matrix entries for all integral equations,
- T_{solve} : the time (secs.) to solve the linear system

Table 1: Results for rectangular 3D cavity at different wavenumber.

k	N_f	N_{pts}	N_{tot}	$T_{matgen}(s)$	$T_{solve}(s)$	E_{error}
1	1	240	600	53.5	0.12	$2 \cdot 10^{-14}$
10	1	240	600	80.9	0.12	$5 \cdot 10^{-9}$
10	41	240	600	176	0.25	$4 \cdot 10^{-9}$
20	1	480	1200	329.4	1.4	$6 \cdot 10^{-7}$
20	41	480	1200	602.5	1.5	$4 \cdot 10^{-7}$
40	1	960	2400	1918.9	18.9	$5 \cdot 10^{-6}$
40	41	960	2400	3545.9	18.4	$2 \cdot 10^{-5}$

- E_{error} : the relative L^2 error measured at a few random points inside the cavity.

All experiments were implemented in FORTRAN 90 and carried out on an Intel Xeon 2.5GHz workstation with 60 cores and 1.5 terabytes of memory. We made use of OPENMP for parallelism across decoupled Fourier modes, and simple block LU-factorization using LAPACK for matrix inversion. Various fast direct solvers such as [19, 26, 29, 34] could be applied if larger problems were involved, no effort was made to further accelerate our code.

Example 1

We first consider a cavity with rectangular cross section (Fig. 4a). The depth and radius of the cavity are both set to 1. We solve the test problem described above at several wavenumbers, with accuracy results shown in Table 1. Note that the CPU time is dominated by the computation of matrix elements, which scales quadratically with the number of unknowns. Because distinct Fourier modes are uncoupled, the solution of the various linear systems is embarrassingly parallel and, for the problem sizes considered, does not dominate the cost despite the asymptotic $O(N_{pts}^3)$ scaling. Note also that the accuracy is very high at low wavenumbers, and slowly deteriorates at higher wavenumber. This is due largely to the corner singularities in the density \mathbf{M} , which are stronger with increasing wavenumber. Additional refinement is necessary if higher accuracy were required. The scattering field for plane wave incidence at $k = 10$ is given in Fig. 4b with 41 modes.

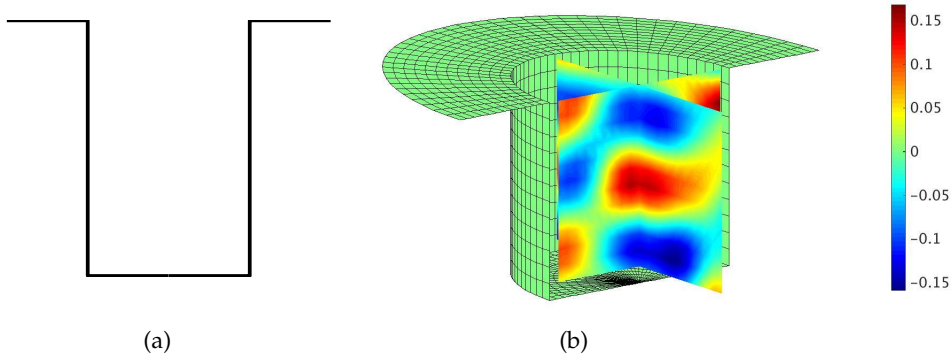


Figure 4: Result for example 1. (a) Cross section of the cavity. (b) Real part of the scattered electrical field E_x at $k = 10$ from a plane wave incidence.

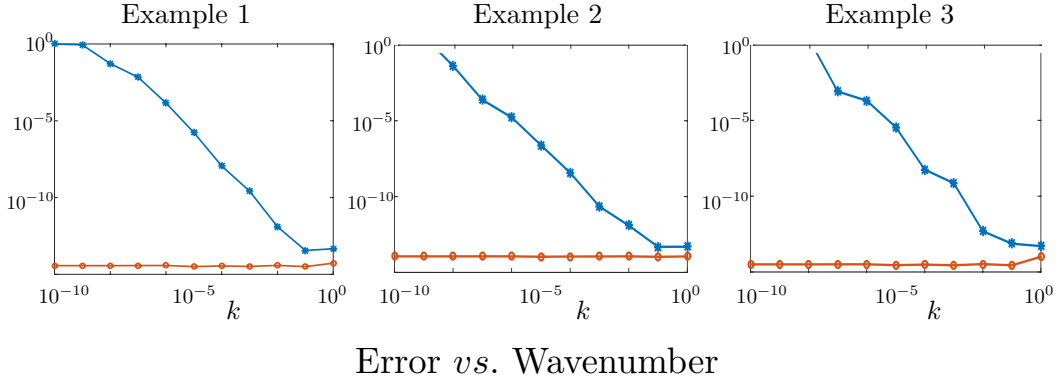


Figure 5: Illustration of low-frequency breakdown in the electric field. For Examples 1-3, the lower curve (red) shows the error of the solution obtained from (4.13) as a function of k and the upper curve (blue) shows the error of the solution obtained from solving (2.23).

Results in Table 1 are obtained through solving eq. (2.23), without the low-frequency stabilization of eq. (4.13) for $k \geq 1$. In Fig. 5, we show the difference in using (2.23) or (4.13) as $k \rightarrow 0$. Low-frequency breakdown is clearly manifested in the original formulation, while (4.13) remains stable.

Example 2

For our second example, we consider the cavity whose generating curve (Fig. 6a) is given by

$$\begin{aligned} r(s) &= [1 - 0.1 \sin(6\pi s)] \sin\left(\frac{\pi}{2}s\right), \\ z(s) &= -[1 - 0.1 \sin(6\pi s)] \cos\left(\frac{\pi}{2}s\right), \end{aligned} \tag{6.3}$$

for $s \in [0, 1]$. The incoming field is again generated by the loop source as stated at the beginning of this section. Accuracy results are provided in Table 2 for various wavenumbers. A sufficient number of points is used to obtain high accuracy at all wavenumbers, with the computational cost again dominated by T_{matgen} . Fig. 6b shows the plane wave scattering at $k = 10$ with 41 modes. We also compare the behavior of eqs. (2.23) and (4.13) in terms of low-frequency breakdown (Fig. 5) and see the advantages of (4.13) as $k \rightarrow 0$.

Table 2: Numerical results for the cavity of Example 2 at various wavenumbers.

k	N_f	N_{pts}	N_{tot}	$T_{matgen}(s)$	$T_{solve}(s)$	E_{error}
1	1	360	960	112.0	0.5	$4 \cdot 10^{-15}$
10	1	360	960	138.4	0.5	$5 \cdot 4^{-13}$
10	41	360	960	273.4	0.5	$5 \cdot 10^{-13}$
20	1	720	1920	578.8	9.3	$4 \cdot 10^{-12}$
20	61	720	1920	1237.5	12.3	$4 \cdot 10^{-12}$
40	1	1440	3840	4068.7	134.5	$5 \cdot 10^{-11}$
40	81	1440	3840	9137.6	145.1	$7 \cdot 10^{-11}$

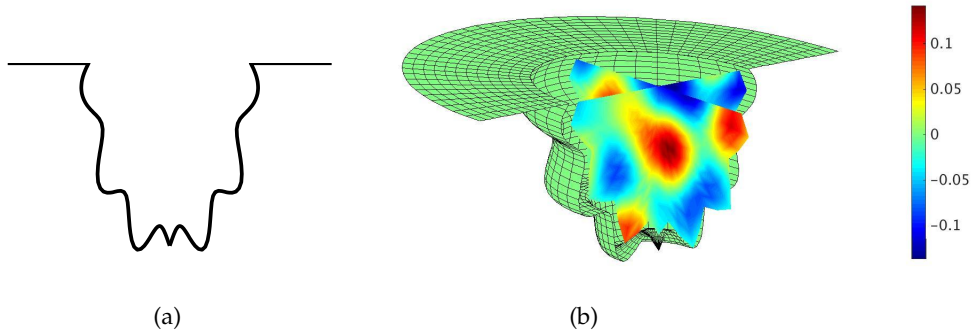


Figure 6: Results for Example 2. (a) Cross section of the cavity. (b) Real part of the scattered electric field E_x at $k = 10$ from a plane wave incidence.

Example 3

For our final example, we consider the cavity generated by a polygonal curve whose vertex coordinates are given by

$$V = \{(0, -0.5), (0.5, -0.5), (0.5, -0.7), (0.25, -0.7), (0.25, -1), (1, -1), (1, 0)\}, \quad (6.4)$$

see Figure 7a.

We employ dyadic refinement on each segment to resolve the various corner singularities. Results are shown in Table 3, with accuracies given by comparison with the exact data. For plane wave incidence at $k = 10$, Fig. 7b gives the scattered field. The low-frequency behavior is illustrated in Fig. 5, which shows the advantage of equation (4.13) again.

7 Conclusions

In this paper, we have developed a new integral representation for the problem of scattering from a three-dimensional cavity embedded in a perfectly conducting half-space which leads to a well

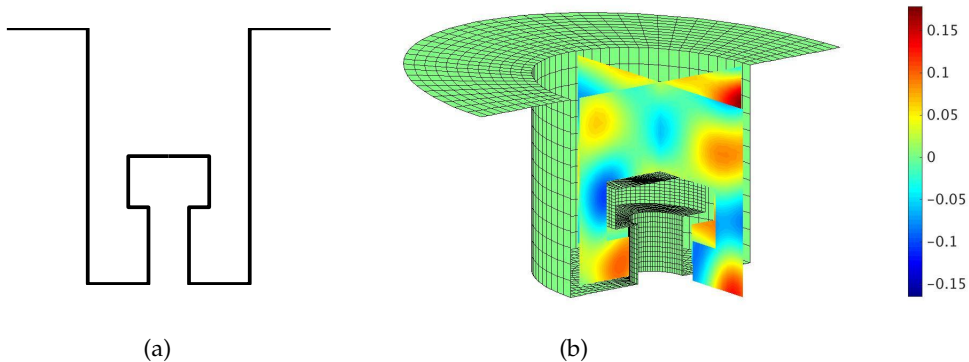


Figure 7: Results for Example 3. (a) Cross section of the cavity. (b) Real part of the scattered electrical field E_x for $k = 10$ from a plane wave incidence.

Table 3: Numerical results for the cavity of Example 3 at various wavenumbers.

k	N_f	N_{pts}	N_{tot}	$T_{matgen}(s)$	$T_{solve}(s)$	E_{error}
1	1	480	1080	201.2	0.70	$2 \cdot 10^{-14}$
10	1	480	1080	246.7	0.70	$5 \cdot 10^{-9}$
10	41	480	1080	558.5	0.75	$4 \cdot 10^{-9}$
20	1	960	2160	1217.8	13.9	$6 \cdot 10^{-7}$
20	41	960	2160	2425.8	13.2	$4 \cdot 10^{-7}$
40	1	1920	4320	5252.7	119.6	$5 \cdot 10^{-6}$

conditioned integral equation. The resulting integral equation is resonance free for all wavenumbers k , immune from low-frequency (dense-mesh) breakdown, and we have established existence and uniqueness for its solution. In particular, the resulting linear system is well-conditioned all the way down to the static limit. Furthermore, the solution to this integral equation allows for the accurate reconstruction of the electric field in the limit as $k \rightarrow 0$. However, since inherently the unknowns in our formulation are current-like vector fields, reconstruction of the magnetic field suffers (albeit only mildly) from low-frequency breakdown. In order to overcome this, alternative representations using charge-like variables would have to be developed.

The effectiveness of the scheme was demonstrated in rotationally symmetric cavities using separation of variables in the azimuthal direction, and a subsequent high-order integral equation method on the cavity's generating curve. The solution for each mode involves only line integrals along the generating curve that defines the geometry. This permits the use of efficient generalized Gaussian quadratures and stable, adaptive mesh refinement into the geometric singularities. We illustrated the performance of the scheme with several examples.

As discussed in section 4, one open question concerns a mild form of low-frequency breakdown in evaluating the magnetic field. We are presently investigating whether the use of generalized Debye sources [16, 17] can be used to overcome this issue. Furthermore, in the present paper, we have made strong use of axisymmetry in developing a numerical solver. We are working on extending the relevant code to arbitrarily-shaped cavities using fully three-dimensional quadratures on triangulated surfaces.

References

- [1] H. Ammari, G. Bao, and A. W. Wood. An integral equation method for the electromagnetic scattering from cavities. *Math. Meth. Appl. Sci.*, 23:1057–1072, 2000.
- [2] H. Ammari, G. Bao, and A. W. Wood. Analysis of the electromagnetic scattering from a cavity. *Japan J. Indust. Appl. Math.*, 19(2):301–310, 2002.
- [3] H. Ammari, G. Bao, and A. W. Wood. A cavity problem for Maxwell's equation. *Meth. Appl. Anal.*, 9(2):249–260, 2002.
- [4] G. Bao, J. Gao, and P. Li. Analysis of direct and inverse cavity scattering problems. *Numer. Math. Theor. Meth. Appl.*, 4:419–442, 2011.

- [5] G. Bao, J. Gao, J. Lin, and W. Zhang. Mode matching for the electromagnetic scattering from three-dimensional large cavities. *IEEE Antennas Wireless Propag.*, 60:2004–2010, 2012.
- [6] G. Bao and J. Lai. Optimal shape design of a cavity for radar cross section reduction. *SIAM J. Control Optim.*, 52(4):2122–2140, 2014.
- [7] G. Bao and J. Lai. Radar cross section reduction of a cavity in the ground plane. *Commun. Comput. Phys.*, 15:895–910, 2014.
- [8] G. Bao and W. Sun. A fast algorithm for the electromagnetic scattering from a large cavity. *SIAM J. Sci. Comput.*, 27:553–574, 2005.
- [9] G. Bao, K. Yun, and Z. Zhou. Stability of the scattering from a large electromagnetic cavity in two dimensions. *SIAM J. Math. Anal.*, 44(1):383–404, 2012.
- [10] J. Bremer and Z. Gimbutas. A Nyström method for weakly singular integral operators on surfaces. *J. Comput. Phys.*, 231(14):4885–4903, may 2012.
- [11] J. Bremer, Z. Gimbutas, and V. Rokhlin. A nonlinear optimization procedure for generalized Gaussian quadratures. *SIAM J. Sci. Comput.*, 32(4):1761–1788, jun 2010.
- [12] A. Buffa, M. Costabel, and D. Sheen. On traces for $\mathbf{H}(\mathbf{curl}, \Omega)$ in Lipschitz domains. *J. Math. Anal. Appl.*, 276:845–867, 2002.
- [13] R. Burkholder and P. Pathak. Analysis of EM penetration into and scattering by electrically large open waveguide cavities using Gaussian beam shooting. *Proc. IEEE*, 79:1401–1412, 1991.
- [14] H. Cheng, W. Y. Crutchfield, Z. Gimbutas, L. Greengard, F. Ethridge, J. Huang, V. Rokhlin, N. Yarvin, and J. Zhao. A wideband fast multipole method for the Helmholtz equation in three dimensions. *J. Comput. Phys.*, 216(1):300–325, jul 2006.
- [15] D. Colton and R. Kress. *Integral Equation Method in Scattering Theory*. Wiley-Interscience, New York, 1983.
- [16] C. L. Epstein and L. Greengard. Debye Sources and the Numerical Solution of the Time Harmonic Maxwell Equations. *Comm. Pure Appl. Math.*, 63(4):413–463, 2010.
- [17] C. L. Epstein, L. Greengard, and M. O’Neil. Debye Sources and the Numerical Solution of the Time Harmonic Maxwell Equations II. *Comm. Pure Appl. Math.*, 66(5):753–789, 2013.
- [18] S. D. Gedney and R. Mittra. The use of the FFT for the efficient solution of the problem of electromagnetic scattering by a body of revolution. *IEEE Trans. Antennas Propag.*, 38:313–322, 1990.
- [19] A. Gillman, P. M. Young, and P.-G. Martinsson. A direct solver with $O(N)$ complexity for integral equations on one-dimensional domains. *Front. Math. China*, 7(2):217–247, 2012.
- [20] K. L. Greengard, L. Ho and J.-Y. Lee. A fast direct solver for scattering from periodic structures with multiple material interfaces in two dimensions. *J. Comput. Phys.*, 258:738–751, 2014.

- [21] L. Greengard and J.-Y. Lee. Stable and accurate integral equation methods for scattering problems with multiple material interfaces in two dimensions. *J. Comput. Phys.*, 231:2389–2395, 2012.
- [22] S. Hao, A. H. Barnett, P. G. Martinsson, and P. Young. High-order accurate Nyström discretization of integral equations with weakly singular kernels on smooth curves in the plane. *Adv. Comput. Math.*, 40:245–272, 2014.
- [23] S. Hao, P.-G. Martinsson, and P. Young. An efficient and highly accurate solver for multi-body acoustic scattering problems involving rotationally symmetric scatterers. *Comput. Math. Appl.*, 69:304–318, 2015.
- [24] J. Helsing and A. Karlsson. An explicit kernel-split panel-based Nyström scheme for integral equations on axially symmetric surfaces. *J. Comput. Phys.*, 272:686–703, 2014.
- [25] J. Helsing and A. Karlsson. Determination of normalized electric eigenfields in microwave cavities with sharp edges. *arXiv:1506.05717*, 2015.
- [26] K. L. Ho and L. Greengard. A fast direct solver for structured linear systems by recursive skeletonization. *SIAM J. Sci. Comput.*, 34(5):2507–2532, 2012.
- [27] A. Kirsch and F. Hettlich. *The Mathematical Theory of Time-Harmonic Maxwell’s Equations*. Springer Verlag, Cham, Switzerland, 2015.
- [28] A. A. Kucharski. A method of moments solution for electromagnetic scattering by inhomogeneous dielectric bodies of revolution. *IEEE Trans. Antennas Propag.*, 48(8):1202–1210, 2000.
- [29] J. Lai, S. Ambikasaran, and L. F. Greengard. A Fast Direct Solver for High Frequency Scattering from a Large Cavity in Two Dimensions. *SIAM J. Sci. Comput.*, 36(6):B887–B903, 2014.
- [30] P. Li. An inverse cavity problem for Maxwell’s equations. *J. Differ. Equations*, 252(4):3209 – 3225, 2012.
- [31] P. Li, L.-L. Wang, and A. Wood. Analysis of Transient Electromagnetic Scattering from a Three-Dimensional Open Cavity. *SIAM J. Appl. Math.*, 75(4):1675–1699, 2015.
- [32] H. Ling, R. Chou, and S. Lee. Shooting and bouncing rays: Calculating the RCS of an arbitrarily shaped cavity. *IEEE Trans. Antennas Propag.*, 37:194–205, 1989.
- [33] J. Liu and J. Jin. A special higher order finite-element method for scattering by deep cavities. *IEEE Trans. Antennas Propag.*, 48:694–703, 2000.
- [34] Y. Liu and A. H. Barnett. Efficient numerical solution of acoustic scattering from doubly-periodic arrays of axisymmetric objects. *arXiv:1506.05083*, 2016.
- [35] J.-C. Nedelec. *Acoustic and Electromagnetic Equations*. Springer-Verlag New York, 2001.
- [36] M. O’Neil, C. L. Epstein, and L. Greengard. High-order wideband direct solvers for electromagnetic scattering from bodies of revolution. 2016. In preparation.

- [37] C. H. Papas. *Theory of Electromagnetic Wave Propagation*. Dover, New York, NY, 1988.
- [38] C. Pérez-Arancibia and O. P. Bruno. High-order integral equation methods for problems of scattering by bumps and cavities on half-planes. *J. Opt. Soc. Am. A*, 31(8):1738–1746, 2014.
- [39] P. Young, S. Hao, and P. G. Martinsson. A high-order Nyström discretization scheme for boundary integral equations defined on rotationally symmetric surfaces. *J. Comput. Phys.*, 231(11):4142–4159, 2012.
- [40] J.-S. Zhao and W. C. Chew. Integral Equation Solution of Maxwell’s Equations from Zero Frequency to Microwave Frequencies. *IEEE Trans. Antennas Propag.*, 48(10):1635–1645, 2000.